Photocatalyzed Hydrogen Evolution from Water by a Composite Catalyst of NH$_2$-MIL-125(Ti) and Surface Nickel(II) Species

Dr. K. Meyer,[a] S. Bashir,[b] Prof. Dr. J. Llorca,[c] Prof. Dr. H. Idriss,[b] Dr. M. Ranocchiari,*[d] Prof. Dr. J. A. van Bokhoven*[a,d]

[a]   Dr. K. Meyer: Prof. Dr. J. A. van Bokhoven
       Department of Chemistry and Applied Biosciences, Institute for Chemical and Bioengineering, ETH Zürich, Wolfgang-Pauli-Str. 10, CH-8093 Zürich, Switzerland
[b]   S. Bashir, Prof. Dr. H. Idriss
       SABIC, P.O. Box 4545-4700, 23955 Thuwal, Saudi Arabia
[c]   Prof. Dr. Jordi Llorca
       Institute of Energy Technologies and Centre for Research in NanoEngineering, Technical University of Catalonia, Avda. Diagonal 647, 08028 Barcelona, Spain
[d]   Dr. Marco Ranocchiari, Prof. Dr. J. A. van Bokhoven
       Paul Scherrer Institute, 5232 Villigen, Switzerland

Abstract: A composite of the metal—organic framework (MOF) NH$_2$-MIL-125(Ti) and molecular and ionic nickel(II) species catalyzed hydrogen evolution from water under UV light. In 95 v/v% aqueous conditions the composite produced hydrogen in quantities two orders of magnitude higher than that of the virgin framework and an order of magnitude greater than that of the molecular catalyst. In a 2 v/v% water and acetonitrile mixture, the composite demonstrated a TOF of 28 mol H$_2$ g(Ni)$^{-1}$ h^{-1} and remained active for up to 50 h, sustaining catalysis for three times longer and yielding 20-fold the amount of hydrogen. Appraisal of physical mixtures of the MOF and each of the nickel species under identical photocatalytic conditions suggest that similar surface localized light sensitization and proton reduction processes operate in the composite catalyst. Both nickel species contribute to catalytic conversion, although different activation behaviors are observed.

Introduction

Photocatalytic hydrogen production capitalizes on the renewable energy feedstocks water and sunlight. Hydrogen is the most efficient energy carrier known and plays a crucial role in the chemical industry. Many semiconductor materials, such as titania, sustain UV-promoted water splitting in the presence of metals.[1] Numerous strategies have been developed to improve the efficiency of hydrogen producing photocatalysts. These include addition of noble metals (for reduction of protons),[2] metal oxides and phosphates (for oxidation of oxygen ions),[3, 4] light sensitizers (to inject electrons into the conduction band),[5] as well as plasmonic metals (to enhance the internal electric field).[6] Similarly, highly active molecular catalysts such as cobalt-containing cobaloxime,[7] and nickel-based DuBois[8, 9] and pyridine-thiolate[10, 11] catalysts, may be integrated with photoreceptive heterogeneous supports to increase catalytic activity. Catalysts and sensitizers are typically located on the same semiconductor crystallite or occupy multiple interconnected phases, each with specific functionality. In this way phosphonate functionalized cobaloxime tethered to P25 titania achieved a TOF of 4.2 µmol H$_2$ h^{-1} in pH-neutral water under UV-visible light (150 W, 100 mW cm^{-2}) with the aid of sacrificial donor triethanolamine.[12] Analogously, a phosphonic acid functionalized [Ru(bpy)$_3$]$^{2+}$ light sensitizer activated an efficient DuBois-type catalyst attached to P25 titania, attaining a TOF of 72 h^{-1}.[13]

Metal–organic frameworks (MOFs) assembled from metal-oxygen clusters and organic linkers are widely known for their large internal surface area and propensity for reversible uptake of small molecules.[14, 15] MOFs have found application in environmentally significant catalytic processes such as formic acid dehydrogenation,[16-18] photocatalyzed carbon dioxide reduction[19, 20] and organic transformations,[21, 22] as well as water oxidation and reduction.[23] NH$_2$-MIL-125(Ti), constructed from Ti$_8$O$_8$ clusters and light absorbing aminoterephthalic acid linkers (with 350 and 550 nm absorption maxima) generated 500 µmol of H$_2$ g(catalyst)$^{-1}$ after 3 h of visible light irradiation (500 W). EPR measurements revealed that Ti^{4+} cluster ions are reduced to Ti^{3+} upon visible light irradiation, indicating injection of electrons sourced from the photoexcited organic linker into the Ti$_8$O$_8$ cluster.[24] Numerous studies have since attempted to augment the activity of the original system by addition of noble metals[25] and semiconductors.[26] A cobaloxime molecular complex physisorbed onto NH$_2$-MIL-125(Ti) generated hydrogen when a 2 v/v% water and acetonitrile suspension of the composite was illuminated under visible light (500 W, 883.6 µmol(photons) s^{-1} m^{-2} between 350-455 nm) in the presence of a sacrificial donor. In contrast to the pure MOF, Ti^{3+} was not detected by EPR spectroscopy. Evolution of a Co^{2+} species was observed instead, suggesting that the titanium-containing MOF and cobalt-containing complex are part of a rapid electron transport chain terminating with a proton reducing cobaloxime catalyst.[27]

Results and Discussion

Herein we describe the assembly, characterization and activity of a NH$_2$-MIL-125(Ti) composite containing a highly active proton reducing nickel(II) catalyst[10] Ni(dmobpy)(2-mpy)$_2$ (dmobpy = 4,4'-dimethoxy-2,2'-bipyridine, 2-mpy = 2-mercaptopyridyl). Our catalyst is the first of its type containing nickel, and is one of only a handful of MOF composites that supports collaborative proton reduction between a photoreceptive MOF and a molecular-type hydrogen evolving catalyst. The Ni@NH$_2$-MIL-125(Ti) composite was prepared by stepwise room temperature introduction of Ni(dmobpy)(2-mpy)$_2$ precursors into the pre-formed MOF (Figure 1). The dmobpy

ligand was added to an acetonitrile suspension of NH_2-MIL-125(Ti) and $Ni(NO_3)_2 \cdot 6H_2O$, followed by pyridine-2-thiolate prepared from 2-mercaptopyridine and triethylamine.
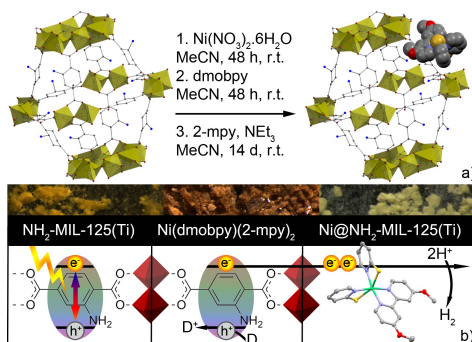

Figure 1. a) Stepwise assembly of Ni@NH_2-MIL-125(Ti). Ni(dmobpy)(2-mpy)$_2$ is shown in spacefill mode for clarity. b) Schematic depicting photoexcitation of the aminoterephthalic acid linker, relay of photoexcited electrons to titanium oxide clusters and subsequent proton reduction mediated by the molecular catalyst. Adapted with permission of Ref. 23, 2015, Royal Society of Chemistry.

Atomic absorption spectroscopy carried out on nitric acid digested portions of Ni@NH_2-MIL-125(Ti) confirmed a 1.4 ± 0.1 wt.% loading of nickel relative to the total weight of the composite. Due to this low loading d-d transitions at 450-800 nm and infrared stretches corresponding to Ni(dmobpy)(2-mpy)$_2$ (Supporting Information, Figure S1 and S2) are not clearly visible in the composite material. However, absorption maxima arising from π-π* intra-ligand transitions of the framework are slightly UV-shifted for Ni@NH_2-MIL-125(Ti) (484 nm absorption edge) relative to NH_2-MIL-125(Ti) (520 nm absorption edge).

^{1}H NMR digestion experiments also support formation of Ni(dmobpy)(2-mpy)$_2$ within the composite, revealing the anticipated 1:2 dmobpy and 2-mpy aryl integral ratios and corresponding chemical shift positions (Supporting Information, Figure S3a and b). The constrictive 5-7 Å apertures of the virgin MOF prevent diffusion of pre-formed nickel complex into the 12.55 Å diameter internal cavities of the framework, and likely restrict assembly of the complex to the surface of MOF crystals because of the bulky nature of the dmobpy molecule (4.753(5) x 6.932(5) Å).[27] Both virgin MOF and Ni@NH_2-MIL-125(Ti) are characterized by similar type-II nitrogen adsorption isotherms. The BET value of Ni@NH_2-MIL-125(Ti) was reduced with respect to virgin NH_2-MIL-125(Ti), dropping from about 1400 to 910 m^2/g, and an accompanying constriction of total pore volume from 0.68 to 0.48 cm^3/g was observed (Supporting Information, Figure S4 and Table S1). Powder X-ray diffraction (PXRD) studies support retention of the original NH_2-MIL-125(Ti) framework topology after impregnation (Supporting Information, Figure S5) and we did not observe Bragg reflections distinctive for titania rutile ((110) plane at 27.5°) or anatase ((101) plane at 25.2°) in the virgin MOF or Ni@NH_2-MIL-125(Ti). The TEM images of the composite, revealed a globular structure with an internal layered morphology (Figure 2). Layers are not stacked and their thickness is about 9.0 Å. This value is obtained by both direct lattice fringe analysis as well as by the spots recorded in the Fourier Transform (FT) images of selected areas (Figure 2a). The observed spacing is consistent with that obtained by PXRD for NH_2-MIL-125(Ti), corresponding to the X-ray diffraction line at 2θ = 9.76° (dhkl value 9.05 Å). Both at low and high magnification the morphology of the sample is very homogeneous, comprising small ordered domains. It was not possible to locate the position of the nickel atoms in the MOF; it is important to highlight that the absence of nickel particles in these images indicate its presence in sub-nanometric dimensions.
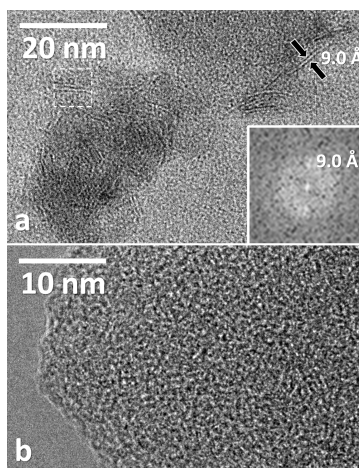

Figure 2. HRTEM images of Ni@NH_2-MIL-125(Ti). a) The FT image obtained from the area enclosed in the white square, which shows spots at 9.0 Å; and b) the FT image after two-fold magnification.

We sought to better understand the chemical composition of the Ni@NH$_2$-MIL-125(Ti) composite using X-ray near edge spectroscopy (XANES). Nickel K-edge XANES was used to ascertain the nature of nickel(II) species associated with Ni@NH$_2$-MIL-125(Ti) using Ni(NO$_3$)$_2$.6H$_2$O and the Ni(dmobpy)(2-mpy)$_2$ complex as standards (Figure 3). We considered penetration of small 4.053(4) Å diameter Ni(NO$_3$)$_2$.6H$_2$O species into the pores of NH$_2$-MIL-125(Ti) during composite preparation, thus contributing to the total amount of nickel present in the composite material. Linear combination fitting of the Ni K-edge XAS spectra carried out in ATHENA[28] revealed an approximately 49:48 split between ionic and molecular species, with a 3% contribution from unknown species (deconvolution of the fitting is provided in the Supporting Information, Table S2 and Figure S6). We rationalize that once Ni(NO$_3$)$_2$.6H$_2$O migrates into the porous MOF it becomes resistant to removal by washing because it is 1) waylaid by charge-balancing nitrate ions, and 2) pore obstruction by the larger molecular complex (10.796(4) x 10.552(4) x 4.898(1) Å)[10] prevents egress out of the constricted MOF pores. Notably, Gascon et al. detect residual cobalt salts in a related cobaloxime MOF composite with NH$_2$-MIL-125(Ti).[29]
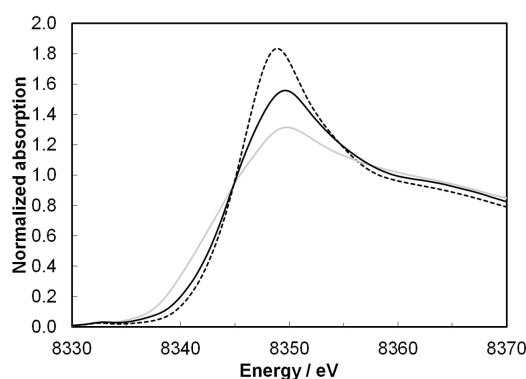

Figure 3. XANES spectra of Ni(dmobpy)(2-mpy)$_2$ (gray), Ni@NH$_2$-MIL-125(Ti) (black) and Ni(NO$_3$)$_2$.6H$_2$O (dashed), depicting the pre-edge region and changes in white line intensity, edge position, and line broadening.

Inspection of the nickel K-edge XANES spectra of Ni@NH$_2$-MIL-125(Ti) reveals a low intensity pre-edge feature around 8332 eV, which is typical of the 1s to 3d transition in octahedral nickel.[30] The spectra of each sample presents a white line position around 8350 eV, distinctive for nickel(II).[31] Intensity of the white line arises from multiple scattering processes,[32] and is known to be suppressed by distortions to octahedral coordination geometry.[30] Consequently, a low intensity white line is observed for Ni(dmobpy)(2-mpy)$_2$ while that for Ni@NH$_2$-MIL-125(Ti) is intermediate between the molecular complex and symmetric hexaaqua coordinated nickel nitrate. Peak broadening observed at the white line positions of Ni(NO$_3$)$_2$.6H$_2$O, Ni(dmobpy)(2-mpy)$_2$, and Ni@NH$_2$-MIL-125(Ti) is explained by average ligand hardness. The edge energy moves to lower values and the slope of the edge decreases in the case of soft ligands, such as sulfur coordination to nickel.[33] The ligand environment of Ni(NO$_3$)$_2$.6H$_2$O is composed of the hard Pearson's Lewis bases water and nitrate. By comparison, the average ligand hardness of Ni(dmobpy)(2-mpy)$_2$ lies somewhere between intermediate and soft because the nickel coordination sphere comprises bipyridine and mercaptopyridyl Pearson's Lewis bases. The expected trends in white line positions and absorption edge gradients are played out in the data, with Ni@NH$_2$-MIL-125(Ti) occupying a position in between the ionic and molecular nickel standards. These observations further support a roughly 1:1 ratio of nickel nitrate and Ni(dmobpy)(2-mpy)$_2$ in the composite.

X-ray photoelectron spectroscopic (XPS) analysis was carried out on NH$_2$-MIL-125(Ti) and Ni@NH$_2$-MIL-125(Ti) (Figure 4). XPS lines of Ni2p, Ti2p, S2p, N1s, O1s, and C1s were collected, in addition to the valence band, for samples in their as-prepared state and after reduction by argon ions. Sputtering experiments allowed insightful assignment of peaks to be made by demonstrating the ease of reduction of metal cations, and probing surface versus bulk contributions arising from Ni@NH$_2$-MIL-125(Ti)–a complex and porous structure within which ligand contributions influence signal attenuation and may affect binding energy positions. In the valence band region the Ar$^+$ sputtered Ni@NH$_2$-MIL-125(Ti) surface developed approximately 1.5 eV below the Fermi level due to d electrons of both titanium and surface nickel atoms formed upon reduction of the corresponding metal cations (Supporting Information, Figure S7).[34] XPS Ni2p lines are displayed in Figure 4, where doublet peaks at 854.1 and 856.1 eV (Ni2p$_{3/2}$), as well as 874.1 and 871.6 eV (Ni2p$_{1/2}$) are associated with a Ni^{2+} species residing on the fresh surface. We attribute the multiplet nature of these peaks to ligand effects on Ni^{2+}, duly noting that multiplicity is commonly observed for Ni^{2+} cations.[35] In comparison, previously studied Ni(II)O/TiO$_2$ surfaces present typical Ni2p doublet peaks at 873.2 (Ni2p$_{1/2}$) and 855.6 eV (Ni2p$_{3/2}$).[36] Pure nickel sulfide is metallic, and is consequently not a useful reference for Ni^{2+} contained in Ni@NH$_2$-MIL-125(Ti). However, it is worth noting that the Ni2p of nickel sulfide differs little from that of nickel metal, with a slightly higher binding energy shift of about 0.5 eV. Upon ion sputtering of Ni@NH$_2$-MIL-125(Ti) one peak was seen at each split indicative of the formation of nickel metal. The Ni2p$_{1/2}$ and Ni2p$_{3/2}$ lines at 871.0 and 853.5 eV, respectively, are similar to those measured for an Ar$^+$-sputtered nickel foil.[37] Weak peaks about 5.7 eV above the Ni2p peaks of sputtered samples are assigned to surface plasmon loss features.[38] Notably, overall signal intensity increases with sputtering due to a change in cross-section between Ni^0 and Ni^{2+} and as a consequence of ligand removal (molecular screening effect). The considerable increase of Ni2p lines upon Ar$^+$ sputtering (ligand removal) indicate the large number of nickel atoms on the

surface and in the pores of the MOF, and give further support for a highly dispersed compound. The Ti2p spectra observed are typical of Ti^{4+} cations, displaying $Ti2p_{3/2}$ and $Ti2p_{1/2}$ lines at 459.3 and 464.6 eV, respectively (Figure 4). Interestingly, argon sputtering reduction of Ti^{4+} in the composite does not match the behavior of titanium cations in titania,[39] but shows an additional distinct contribution from a preferentially formed compound. A 3 eV discrepancy in binding energy between fresh and sputtered species indicates a greater than one oxidation state increase. The distinct position of the peak at about 456.2 eV can be attributed to a Ti^{+2} oxidation state. The unusual preferential formation of Ti^{+2}, when compared to reduced TiO_2 (in which non-selective reduction occurs),[39] might be linked to the ease by which the Ti-O-C moiety of the framework is reduced; relatively facile reduction is posited for Ti-O sites in the MIL-125(Ti) framework compared to those in TiO_2.[40] This property is replicated by the virgin MOF. Inspection of the N1s spectra similarly indicate an approximately 3 eV shift from an N1s sp^3-type nitrogen (around 400 eV; Supporting Information, Figure S8). It is possible that a titanium-nitride species is formed upon ion sputtering.[41] The XPS spectra for S2p (Supporting Information, Figure S8) are typical for transition metal bound mercaptopyridyl[42] and nickel-thiol[43] complexes, displaying two broad peaks at 163.8 and 162.3 eV pertaining to $S2p_{1/2}$ and $S2p_{3/2}$, respectively. A broad signal centered around 169.1 eV in the fresh sample likely arises due to oxidized sulfur species at the surface.[44, 45]
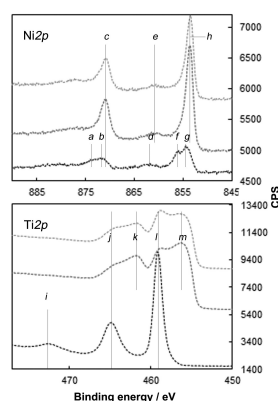

Figure 4. Ni2p and Ti2p band energies derived from Ni@NH₂-MIL-125(Ti) measured after 0 (lowest), 5 (middle) and 10 (top-most) minutes of argon sputtering. Levels: Ni2p a) 874.1, b) 871.6, c) 871, d) 861.6, e) 860.8, f) 856.1, g) 854.1, h) 853.5 eV; Ti2p i) 472.3, j) 464.6, k) 461.8, l) 459.3, m) 456.2 eV. Note: only a part of the satellite structure is shown for Ti2p.

Having established the essential characteristics of the composite, the activity of Ni@NH₂-MIL-125(Ti) as a hydrogen evolving photocatalyst was evaluated against that of NH₂-MIL-125(Ti) and Ni(dmobpy)(2-mpy)₂. Each of the materials was independently suspended in a 5 v/v% triethylamine/ water solution and an inert and light-free environment established before irradiation with a 100 W UV lamp (360 nm, flux of ca. 5 mW/cm²). Evolved gases were monitored over time by gas chromatography. While both NH₂-MIL-125(Ti) and Ni(dmobpy)(2-mpy)₂ deactivate after 300 min under these conditions, the MOF composite offered an approximately 1800-fold improvement on the hydrogen production activity of the virgin MOF (normalized to the weight percent of nickel), attaining 24.8 turnovers and a TOF of 5.0 h⁻¹ after 5 h (Supporting Information, Figure S9a and Table S3). Ni(dmobpy)(2-mpy)₂ (2 mg, representing 11.85 wt.% nickel) yielded an order of magnitude less hydrogen in the absence of the MOF photosensitizer. Ni@NH₂-MIL-125(Ti) activity plateaus after about 1000 min in the predominantly aqueous reaction matrix (Supporting Information, Figure S9b).
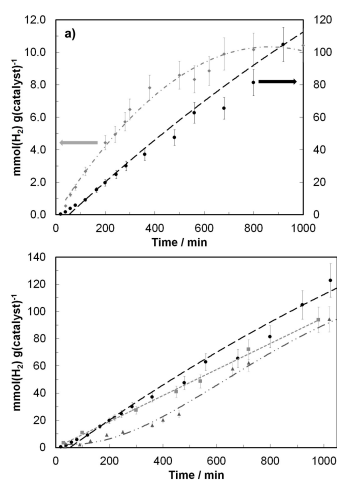

Figure 5. UV photocatalyzed hydrogen production. a) Ni@NH₂-MIL-125(Ti) (2 mg) with 5 v/v% triethylamine/water (left y-axis, grey) and 79:19:2 v/v% acetonitrile/triethylamine/water (right y-axis, black). b) 79: 19: 2 v/v% acetonitrile/triethylamine/water; Ni@NH₂-MIL-125(Ti) (●), mixture of Ni(dmobpy)(2-mpy)₂ and NH₂-MIL-125(Ti) (■, **Mixture A**), mixture of Ni(NO₃)₂.6H₂O and NH₂-MIL-125(Ti) (▲, **Mixture B**).

Seeking to improve the longevity of our system we experimented with a primarily acetonitrile solvent mixture containing 2 v/v% water and 19 v/v% triethylamine. Under these conditions activity of Ni@NH$_2$-MIL-125(Ti) improved 10-fold (Figure 5) and was prolonged for 3000 min, reaching 906 turnovers, and an initial TOF of 28.3 h^{-1} at the 1000 min mark (normalized with respect to the amount of nickel metal; Supporting Information, Figure S9b and Table S4). Pure MOF evaluated under the same conditions produced only traces of hydrogen and the activity of pure Ni(dmobpy)(2-mpy)$_2$ plateaued at 1 mmol H$_2$ g(catalyst)$^{-1}$ after only 300 min.[46] A related cobaloxime and NH$_2$-MIL-125(Ti) catalytic composite tested under visible light using the same matrix, generated an order of magnitude less hydrogen after 1000 min, and reached only 52 TONs after 65 h (Supporting Information, Table S4).[29]

To elucidate the origin of nickel species responsible for proton reduction, photocatalytic experiments were conducted using mechanical mixtures of solid Ni(dmobpy)(2-mpy)$_2$ and MOF (**Mixture A**), as well as solid Ni(NO$_3$)$_2$.6H$_2$O and MOF (**Mixture B**). Each mixture contained a 0.7 wt% nickel loading, in accordance with the aforementioned XANES and AAS data. **Mixture A** initially elicited activity very similar to that of the composite, suggesting that catalysis mediated by the composite is dependent on Ni(dmobpy)(2-mpy)$_2$ molecules located at the surface of MOF particles (Figure 5b). Activation of the molecule after collision with the photoexcited MOF is therefore likely, resulting in electron transfer to the molecular nickel catalyst (Figure 1). Mechanistic details for proton reduction mediated by the complex in a homogeneous setting are described elsewhere.[10, 47] Hydrogen production induced by **Mixture A** declines after 400 min, and is possibly explained by deactivation of Ni(dmobpy)(2-mpy)$_2$ as a consequence of 2-mpy dissociation and reduction to form 2-mercaptopyridine (HS-C$_5$H$_4$N), or irreversible associations with the surface of the MOF (coordination of the amino group of the MOF linker to an exposed nickel center is a possible pathway, for example). In view of the test with **Mixture B** (Figure 5b), reduction of Ni(dmobpy)(2-mpy)$_2$ into Ni^0 nanoparticles cannot be construed as a deactivation pathway. After a long induction period **Mixture B** elicits efficient hydrogen production, eventually attaining activity on a par with the composite material (Figure 5b; Supporting Information, Figure S9c). A photoreduction process is deemed responsible for reducing Ni(NO$_3$)$_2$ into metallic nickel, a phenomenon that is widely observed upon *in situ* photoreduction of metal oxides or their precursors on substrates, leading to deposition of metal nanoparticles.[48, 49, 36] A composite catalyst formed by slow diffusion of Ni(NO$_3$)$_2$ into NH$_2$-MIL-125(Ti) over two weeks (that is, a composite in which Ni(NO$_3$)$_2$ was given time to permeate into the MOF without encountering the ligating restraints of dmobpy and 2-mpy ligands) contained 4.5 wt% nickel by AAS. Interestingly, under photocatalytic conditions this material and **Mixture B** demonstrated very similar catalytic behavior (Supporting Information, Figure S10), suggesting that photocatalysis originating from reduced Ni(NO$_3$)$_2$ is very likely to be limited to the surface layers of the MOF.

The composite catalyst Ni@NH$_2$-MIL-125(Ti) evidently benefits from the catalytic contributions of two distinct nickel species within the first 50 h of activity, and subsequently deactivates. Photocatalyzed proton reduction in a 95 v/v% aqueous mixture carried out by NH$_2$-MIL-125(Ti), a proton reducing catalyst in its own right,[24] also exhibits deactivation (Supporting Information, Figure S11), suggesting that decline of the composite catalyst may be associated with the MOF itself, and is certainly exacerbated in primarily aqueous media (Supporting Information, Figure S9b). A recent computational paper determined that photoreduction of the MIL-125(Ti) framework is energetically feasible via two pathways, extrinsic reduction with reductants such as hydrogen, or intrinsic reduction by oxygen loss.[40] The latter process would produce irreversible framework defects that subtly alter the band gap and charge transfer properties within the surface layers of the MOF, potentially leading to deactivation of a composite catalyst such as Ni@NH$_2$-MIL-125(Ti). Combatting such an effect might be reasonably achieved using other titanium-themed MOFs (e.g. NTU-9)[50] in which such processes are less favorable.

Conclusions

In summary, we have prepared a composite of NH$_2$-MIL-125(Ti) and a molecular Ni(dmobpy)(2-mpy)$_2$ catalyst by stepwise assembly of the complex in the presence of the MOF. Under preparative conditions a small quantity of Ni(NO$_3$)$_2$ starting material remains trapped in the MOF, as determined by Ni K-edge XANES. The resultant composite generates appreciable quantities of hydrogen under UV light, well in excess of that evolved by other photocatalytically activated MOF molecular composites reported, and it remains active for up to 50 h. Catalytic studies using mechanically mixed versions of the composite indicate that proton reduction occurs at the surface of the MOF. Furthermore, over the course of the composite catalyst's lifetime different nickel species were observed to take center stage. Within the first 1000 min Ni(dmobpy)(2-mpy)$_2$ promotes hydrogen production efficiently, during which Ni(NO$_3$)$_2$ is reduced into catalytically active elemental nickel. Plans are underway to investigate the mechanistic details of this compelling composite system, which showcases the utility of NH$_2$-MIL-125(Ti) as a robust photoactive support for hydrogen evolution from water.

Acknowledgements

[1]   A. Fujishima, K. Honda, *Nature*, **1972**, *238*, 37.
[2]   Z. H. N. Al-Azri, W.-T. Chen, A. Chan, V. Jovic, T. Ina, H. Idriss, G. I. N. Waterhouse, *J. Catal.*, **2015**, *329*, 355-367.
[3]   S. Chen, S. Shen, G. Liu, Y. Qi, F. Zhang. C. Li, *Angew. Chem. Int. Ed.*, **2015**, *54*, 3047-3051.
[4]   J. W. Ager, M. R. Shaner, K. A. Walczak, I. D. Sharp, S. Ardo, *Energy Environ. Sci.*, **2015**, *8*, 2811-2824.
[5]   E. Bae, W. Choi, *J. Phys. Chem. B*, **2006**, *110*, 14792-14799.
[6]   G. I. N. Waterhouse, A. K. Wahab, M. Al-Oufi, V. Jovic, D. H. Anjum, D. Sun-Waterhouse, J. Llorca, H. Idriss, *Scientific Reports*, **2013**, *3*, 2849.
[7]   P.-A. Jacques, V. Artero, J. Pécaut, M. Fontecave, *Proc. Nat. Acad. Sci.*, **2009**, *106*, 20627-20632.
[8]   A. D. Wilson, R. H. Newell, M. J. McNevin, J. T. Muckerman, M. Rakowski DuBois, D. L. DuBois, *J. Am. Chem. Soc.*, **2006**, *128*, 358-366.
[9]   M. L. Helm, M. P. Stewart, R. M. Bullock, M. R. DuBois, D. L. DuBois, *Science*, **2011**, *333*, 863-866.
[10]   Z. Han, L. Shen, W. W. Brennessel, P. L. Holland, R. Eisenberg, *J. Am. Chem. Soc.*, **2013**, *135*, 14659-14669.
[11]   A. Das, Z. Han, W. W. Brennessel, P. L. Holland, R. Eisenberg, *ACS Catal.*, **2015**, *5*, 1397-1406.
[12]   F. Lakadamyali, E. Reisner, *Chem. Commun.*, **2011**, *47*, 1695-1697.
[13]   M. A. Gross, A. Reynal, J. R. Durrant, E. Reisner, *J. Am. Chem. Soc.*, **2014**, *136*, 356-366.
[14]   J. L. C. Rowsell, O. M. Yaghi, *Micropor. Mesopor. Mat.*, **2004**, *73*, 3-14.
[15]   L. J. Murray, M. Dinca, J. R. Long, *Chem. Soc. Rev.*, **2009**, *38*, 1294-1314.
[16]   M. Martis, K. Mori, K. Fujiwara, W.-S. Ahn, H. Yamashita, *J. Phys. Chem. C*, **2013**, *117*, 22805-22810.
[17]   H. Dai, N. Cao, L. Yang, J. Su, W. Luo, G. Cheng, *J. Mat. Chem. A*, **2014**, *2*, 11060-11064.
[18]   A. Beloqui Redondo, F. L. Morel, M. Ranocchiari, J. A. van Bokhoven, *ACS Catal.*, **2015**, *5*, 7099-7103.
[19]   D. Wang, R. Huang, W. Liu, D. Sun, Z. Li, *ACS Catal.*, **2014**, *4*, 4254-4260.
[20]   Y. Fu, D. Sun, Y. Chen, R. Huang, Z. Ding, X. Fu, Z. Li, *Angew. Chem. Int. Ed.*, **2012**, *51*, 3364-3367.
[21]   T. Zhang, W. Lin, *Chem. Soc. Rev.*, **2014**, *43*, 5982-5993.
[22]   M. Ranocchiari, J. A. van Bokhoven, *PhysChemChemPhys*, **2011**, *13*, 6388-6396.
[23]   K. Meyer, M. Ranocchiari and J. A. van Bokhoven, *Energy Environ. Sci.*, **2015**, *8*, 1923-1937.
[24]   Y. Horiuchi, T. Toyao, M. Saito, K. Mochizuki, M. Iwata, H. Higashimura, M. Anpo, M. Matsuoka, *J. Phys. Chem. C*, **2012**, *116*, 20848-20853.
[25]   D. Sun, W. Liu, Y. Fu, Z. Fang, F. Sun, X. Fu, Y. Zhang, Z. Li, *Chem. Eur. J.*, **2014**, *20*, 4780-4788.
[26]   J. He, Z. Yan, J. Wang, J. Xie, L. Jiang, Y. Shi, F. Yuan, F. Yu, Y. Sun, *Chem. Commun.*, **2013**, *49*, 6761-6763.
[27]   M. Dan-Hardi, C. Serre, T. Frot, L. Rozes, G. Maurin, C. Sanchez, G. Férey, *J. Am. Chem. Soc.*, **2009**, *131*, 10857-10859.
[28]   B. Ravel, M. Newville, *Journal of Synchrotron Radiation*, **2005**, *12*, 537.
[29]   M. A. Nasalevich, R. Becker, E. V. Ramos-Fernandez, S. Castellanos, S. L. Veber, M. V. Fedin, F. Kapteijn, J. N. H. Reek, J. I. van der Vlugt, J. Gascon, *Energy Environ. Sci.*, **2015**, *8*, 364-375.
[30]   K. I. Pandya, R. W. Hoffman, J. McBreen, W. E. O'Grady, *Journal of The Electrochemical Society*, **1990**, *137*, 383.
[31]   Wirick, S.; Flynn, G. J.; Sutton, S.; Zolensky, M. E. In Lunar and Planetary Science and Exploration; Inorganic, Organic and Physical Chemistry; NASA Technical Reports: The Woodlands, TX, United States, 2014; Vol. 45th, p 2.
[32]   T. Tanase, R. Nouchi, Y. Oka, M. Kato, N. Nakamura, T. Yamamura, Y. Yamamoto, S. Yano, *J. Chem. Soc., Dalton Trans*. **1993**, 2645.
[33]   G. J. Colpas, M. J. Maroney, C. Bagyinka, M. Kumar, W. S. Willis, S. L. Suib, P. K. Mascharak, N. Baidya, *Inorg. Chem.* **1991**, *30*, 920.
[34]   S. Shabalovskaya, A. Narmonev, O. Ivanova, A. Dementjev, *Phys. Rev. B*, **1993**, *48*, 13296-13311.
[35]   H. W. Nesbitt, D. Legrand, G. M. Bancroft, *Phys. Chem. Min.*, **2000**, *27*, 357-366.
[36]   W.-T. Chen, A. Chan, D. Sun-Waterhouse, T. Moriga, H. Idriss, G. I. N. Waterhouse, *J. Catal.*, **2015**, *326*, 43-53.
[37]   C. D. Wagner, G. E. Muilenberg in *Handbook of x-ray photoelectron spectroscopy: a reference book of standard data for use in x-ray photoelectron spectroscopy*, Physical Electronics Division, Perkin-Elmer Corp., Eden Prairie, Minn. **1979**.
[38]   H. A. E. Hagelin-Weaver, J. F. Weaver, G. B. Hoflund, G. N. Salaita, *J. Electron Spectrosc. Relat. Phenom.*, **2004**, *134*, 139-171.
[39]   H. Idriss, K. G. Pierce, M. A. Barteau, *J. Am. Chem. Soc.*, **1994**, *116*, 3063-3074.
[40]   A. Walsh, C. R. A. Catlow, *ChemPhysChem*, **2010**, *11*, 2341-2344.
[41]   D. Jaeger, J. Patscheider, *J. Electron Spectrosc. Relat. Phenom.*, **2012**, *185*, 523-534.
[42]   H.-L. Zhang, S. D. Evans, J. R. Henderson, R. E. Miles, T. Shen, *J. Phys. Chem. B*, **2003**, *107*, 6087-6095.
[43]   S. A. Best, P. Brant, R. D. Feltham, T. B. Rauchfuss, D. M. Roundhill, R. A. Walton, *Inorg. Chem.*, **1977**, *16*, 1976-1979.
[44]   M. Volmer, M. Stratmann, H. Viefhaus, *Surf. Interface Anal.*, **1990**, *16*, 278-282.
[45]   C. Alonso, M. F. López, A. Gutiérrez, M. L. Escudero, *Surf. Interface Anal.*, **2000**, *30*, 359-363.
[46]   Acetaldehyde, a by-product of hole-scavenging carried out by triethylamine (see: R. F. Bartholomew, R. S. Davidson, *J. Chem. Soc. C*, **1971**, 2342-2346; P. J. DeLaive, B. P. Sullivan, T. J. Meyer, D. G. Whitten, *J. Am. Chem. Soc.*, **1979**, *101*, 4007-4008.), follows non-linear behaviour in all of our experiments (Supporting Information, Figure S12). The discrepancy observed between proportions of acetaldehyde and hydrogen is explained by transformation of the reactive intermediate into other species, as described elsewhere (see Ref. 6).
[47]   Proton reduction mediated by Ni(dmoby)(2-mpy)$_2$ is thought to proceed via a nickel hydride intermediate and reversible coordination and protonation of one of the 2-mercaptopyridyl ligands (forming 2-mercaptopyridinium upon dissociation of the pyridyl group and protonation of the pyridyl nitrogen).
[48]   R. Niishiro, H. Kato, A. Kudo, *PhysChemChemPhys*, **2005**, *7*, 2241-2245.
[49]   R. S. Khnayzer, L. B. Thompson, M. Zamkov, S. Ardo, G. J. Meyer, C. J. Murphy, F. N. Castellano, *J. Phys. Chem. C*, **2012**, *116*, 1429-1438.
[50]   J. Gao, J. Miao, P.-Z. Li, W. Y. Teng, L. Yang, Y. Zhao, B. Liu, Q. Zhang, Chem. Commun., **2014**, *50*, 3786–3788.